Journal of Porphyrins and Phthalocyanines
J. Porphyrins Phthalocyanines 2017; **21**: 1–11
DOI: 10.1142/S1088424617500456

Published at http://www.worldscinet.com/jpp/

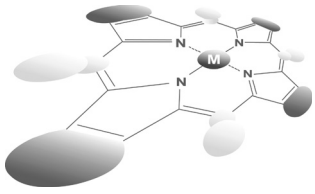

Solvent and substituent effects on UV-vis spectra and redox properties of zinc *p*-hydroxylphenylporphyrins

Guifen Lu*[a,b], Xiaoqin Jiang[b], Zhongping Ou[a,b], Sen Yan[a] and Karl M. Kadish*[b]

[a]*School of Chemistry and Chemical Engineering, Jiangsu University, Zhenjiang 212013, P. R. China*
[b]*Department of Chemistry, University of Houston, Houston, TX 77204-5003, USA*

Received 20 March 2017
Accepted 18 April 2017

ABSTRACT: A series of zinc *p*-hydroxylphenylporphyrins was synthesized and characterized by spectroscopic and electrochemical methods in four different nonaqueous solvents. The investigated compounds are represented as [(*p*-HOPh)$_n$(*p*-*t*BuPh)$_{4-n}$P]Zn, where P represents the dianion of a porphyrin, Ph represents a phenyl group, HO and *t*Bu are *para* substituents on the *meso*-phenyl rings of the macrocycle and n = 0–4. The four utilized nonaqueous solvents were dichloromethane (CH_2Cl_2), *N*,*N*-dimethylformamide (DMF), dimethylsulfoxide (DMSO) and pyridine (Py) which were selected on the basis of their coordinating capabilities. The UV-visible spectra and redox potentials of each porphyrin were analyzed both as a function of Hammett substituent constants for groups at the *para*-positions of the *meso*-phenyl rings and as a function of the Gutmann solvent donor number which is related to the coordinating ability of the solvent. Each porphyrin exhibits two reductions in CH_2Cl_2, DMSO and Py while three reductions are observed in DMF, the additional reaction being due to a phlorin product generated in solution after formation of the porphyrin dianion. Two or three reversible oxidations were seen in CH_2Cl_2, the exact number depending upon the specific porphyrin and the presence of *p*-OH substituents at the *meso*-phenyl rings of the compound. The first two oxidations were assigned as involving the conjugated macrocycle and the third is associated with oxidation of the *meso*-HOPh group(s).

KEYWORDS: zinc *p*-hydroxylphenylporphyrins, synthesis, electrochemistry, solvent effect, substituent effect.

INTRODUCTION

Hydroxyphenyl substituted porphyrins have been used as photosensitizers in model systems for photosynthesis and photodynamic cancer therapy [1–4], as fluorescence probes [5, 6] or as organic functional materials [7–13] in the area of nonlinear optical materials [13] and supramolecular materials [10]. The structural [14–16], spectral [17–19] and electrochemical properties [20–22] for these compounds have been reported, but to the best of our knowledge no laboratory has investigated the UV-visible spectroscopy and electrochemistry of *p*-hydroxyphenyl substituted zinc porphyrins with 0 to 4 hydroxyphenyl groups in different nonaqueous solvents.

This is done in the present paper where a series of *p*-hydroxyphenyl-substituted zinc porphyrins have been synthesized and characterized as to their electrochemical and UV-visible absorption properties in four different nonaqueous solvents. The investigated compounds are shown in Chart 1 and represented by the formula [(*p*-HOPh)$_n$(*p*-*t*BuPh)$_{4-n}$P]Zn, where n = 0–4, P represents the dianion of a porphyrin, HOPh represents a *meso*-hydroxyphenyl group and *t*BuPh, a *meso*-*t*butylphenyl-group on the macrocycle. The four utilized solvents varied from the low-donor and nonbinding solvent CH_2Cl_2 (DN = 0.0) to the higher or stronger coordinating solvents DMF (DN = 26.6), DMSO (DN = 29.8) and pyridine (DN = 33.1) [23]. The binding constants (log*K*) for addition of one solvent molecule to the Zn(II) center

*Correspondence to: Guifen Lu, email: luguifen@ujs.edu.cn, tel: +86 511-88791800, fax: +86 0511-88791800. Karl M. Kadish, email: kkadish@uh.edu, tel: (713) 743-2740, fax: (713) 743-2745

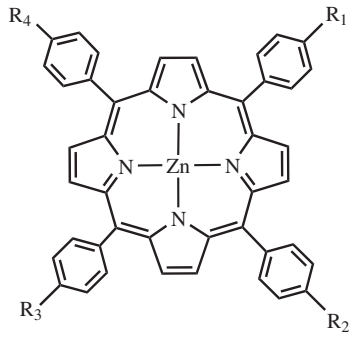

R_1-R_4 = *t*Butyl (**1**)
R_1 = OH, R_2-R_4 = *t*Butyl (**2**)
R_1, R_2 = OH, R_3, R_4 = *t*Butyl (**3**)
R_1-R_3 = OH, R_4 = *t*Butyl (**4**)
R_1-R_4 = OH (**5**)

Chart 1. Structures of investigated zinc porphyrins **1–5**

of the porphyrin were determined using standard equations during specroscopically monitored titrations which were carried out in CH_2Cl_2. Relationships are examined between the solvent binding constants (log*K*) and the Gutmann donor number (DN) of the solvent (S) or the sum of the Hammett substituents constants ($\Sigma\sigma$) of groups at the *para*-position of the *meso*-phenyl rings. The effect of the solvent and number of *meso*-hydroxyphenyl substituents on the electrochemical and spectroscopic properties of the porphyrins is also discussed.

EXPERIMENTAL

Materials and equipment

^{1}H NMR spectra were recorded in a DMSO-d_6 solution at 400 MHz using a Bruker Advance 400 spectrometer at 298 K. Chemical shifts (ppm) were determined with TMS as the internal reference. MALDI-TOF mass spectra were carried out on a Bruker BIFLEX III ultrahigh resolution. Elemental analyses were performed on an Element analyzer FLASH1112A. IR spectra (KBr pellets) were recorded on an AVATAR-370 spectrometer.

Cyclic voltammetry was carried out with an EG&G Model 173 potentiostat or Electrochemical Workstation. A home-made three-electrode cell was used and consisted of a glassy carbon working electrode, a platinum counter electrode and a homemade saturated calomel reference electrode (SCE). The SCE was separated from the bulk of the solution by a fritted glass bridge of low porosity which contained the solvent/supporting electrolyte mixture. All potentials are referenced to the SCE.

Thin-layer UV-visible spectroelectrochemical experiments were performed with a home-built thin-layer cell which has a light transparent platinum-net working electrode. Potentials were applied and monitored with an EG&G model 173 potentiostat. Time-resolved UV-visible spectra were recorded with a Hewlett-Packard model 8453 diode array spectrophotometer. High purity N_2 was used to deoxygenate the solution, and nitrogen was kept over the solution during each electrochemical and spectroelectrochemical experiment.

Determination of binding constants

A series of solutions containing CH_2Cl_2 and different concentrations of DMF, DMSO or Py was prepared and used as a standard titrant. Microliter quantities of the above standard solutions were added gradually to a specially constructed UV-visible cell (path length = 1.0 cm) containing the metalloporphyrin in 6.0 ml CH_2Cl_2. After each addition, the solution was thoroughly mixed and the spectrum was recorded. The changes in spectra were analyzed as a function of the concentration of added solvent, and the Hill equation was used to calculate equilibrium constants (log*K*) as described in the literature [17, 24]. All UV-visible spectral measurements were carried out at room temperature (298 K).

Chemicals

Absolute dichloromethane (CH_2Cl_2), *N*,*N*-dimethylformamide (DMF), dimethyl sulfoxide (DMSO) and pyridine (Py) were received from Aldrich Co. and used as received. High-purity dinitrogen from Trigas was used to deoxygenate the solution before each electrochemical experiment. Tetra-*n*-butylammonium perchlorate (TBAP) was purchased from Fluka Chemika Co. and used without further purification. The investigated zinc porphyrins [(*p*-HOPh)$_n$(*p*-*t*BuPh)$_{4-n}$P]Zn **1–5** were prepared according to literature procedures as described below.

Preparation of [(*p*-HOPh)$_n$(*p*-*t*BuPh)$_{4-n}$P]Zn (1–5)

A mixture of $Zn(CH_3COO)_2 \cdot 2H_2O$ (0.10 mmol) and the free-base porphyrin [(*p*-HOPh)$_n$(*p*-*t*BuPh)$_{4-n}$P]H_2 (0.05 mmol) was added to DMF (6 ml) and heated to 140 °C for 1 h. After cooling the solution to room temperature, the volatiles were removed under reduced pressure, and the residue was chromatographed on a silica gel column with $CHCl_3$ as eluent. A small amount of unreacted free-base porphyrin [(*p*-HOPh)$_n$(*p*-*t*BuPh)$_{4-n}$P]H_2 was eluted as the first fraction, and the target metal porphyrin product was collected as the second fraction. Repeated chromatography followed by recrystallization from $CHCl_3$ and *n*-hexane gave pure purple solid sample of [(*p*-HOPh)$_n$(*p*-*t*BuPh)$_{4-n}$P]Zn **(1–5)**.

[(*p*-*t*BuPh)$_4$P]Zn **1**. Yield: 38.7 mg (86%); ^{1}H NMR (400 MHz, DMSO-d_6): δ 8.78 (s, 8H, β), 8.13 (d, 8H, *o*-Ph), 7.83 (d, 8H, *m*-Ph), 1.58 (s, 36H, *t*bu); MALDI-TOF mass: *calcd* 902.5, *found* 901.8. Elemental analysis

calcd (%) for $ZnC_{60}H_{60}N_4$: C 79.84, H 6.70, N 6.21; *found*: C 79.47, H 6.75, N 6.15.

[(*p*-HOPh)(*p*-*t*BuPh)$_3$P]Zn **2**. Yield: 38.8 mg (90%); ^{1}H NMR (400 MHz, DMSO-d_6): δ 9.86 (s, 1H, OH), 8.84 (d, 4H, β), 8.79 (m, 4H, β), 8.11 (d, 6H, *o*-Ph), 7.97 (d, 2H, *o*-Ph), 7.81 (d, 6H, *m*-Ph), 7.18 (d, 2H, *m*-Ph), 1.57 (s, 27H, *t*bu); MALDI-TOF mass: *calcd* 862.4, *found* 861.6. Elemental analysis *calcd* (%) for $ZnC_{56}H_{52}N_4O$: C 77.99, H 6.08, N 6.50; *found*: C 77.25, H 6.19, N 6.38. Main IR band (cm^{-1}): 3435 (ν O–H).

[*cis*-(*p*-HOPh)$_2$(*p*-*t*BuPh)$_2$P]Zn **3**. Yield: 39.4 mg (96%); ^{1}H NMR (400 MHz, DMSO-d_6): δ 9.86 (s, 2H, OH), 8.84 (d, 4H, β), 8.77 (m, 4H, β), 8.11 (d, 4H, *o*-Ph), 7.97 (d, 4H, *o*-Ph), 7.82 (d, 4H, *m*-Ph), 7.19 (d, 4H, *m*-Ph), 1.58 (s, 18H, *t*bu); MALDI-TOF mass: *calcd* 822.3, *found* 821.1. Elemental analysis *calcd* (%) for $ZnC_{52}H_{44}N_4O_2$: C 75.95, H 5.39, N 6.81; *found*: C 75.78, H 5.39, N 7.07; Main IR band (cm^{-1}): 3453 (ν O–H).

[(*p*-HOPh)$_3$(*p*-*t*BuPh)P]Zn **4**. Yield: 33.6 mg (86%); ^{1}H NMR (400 MHz, DMSO-d_6): δ 9.85 (s, 3H, OH), 8.83 (d, 4H, β), 8.76 (d, 4H, β), 8.12 (d, 2H, *o*-Ph), 7.97 (d, 6H, *o*-Ph), 7.83 (d, 2H, *m*-Ph), 7.18 (d, 6H, *m*-Ph), 1.58 (s, 9H, *t*bu); MALDI-TOF mass: *calcd* 782.2, *found* 781.3. Elemental analysis *calcd* (%) for $ZnC_{48}H_{36}N_4O_3$: C 73.70, H 4.64, N 7.16; *found*: C 73.55, H 4.37, N 7.12; Main IR band (cm^{-1}): 3457 (ν O–H).

[(*p*-HOPh)$_4$P]Zn **5**. Yield: 30.8 mg (83%); ^{1}H NMR (400 MHz, DMSO-d_6): δ 9.85 (s, 4H, OH), 8.80 (s, 8H, β), 7.96 (d, 8H, *o*-Ph), 7.18 (d, 8H, *m*-Ph); MALDI-TOF mass: *calcd* 741.3, *found* 742.1. Elemental analysis *calcd* (%) for $ZnC_{44}H_{28}N_4O_4$: C 71.21, H 3.80, N 7.55; *found*: C 71.55, H 3.73, N 7.39; Main IR band (cm^{-1}): 3298 (ν O–H).

RESULTS AND DISCUSSION

Synthesis

Standard procedures were employed to metalate each free-base porphyrin with a Zn(II) salt to give the zinc porphyrins **1–5** [25]. The reaction workup was facile and afforded the products in a yield of 83–96%.

The composition of each synthesized porphyrin was confirmed by MALDI-TOF mass spectrometry. The molecular ion [M]$^+$ peak was observed in the spectrum of each compound, and satisfactory elemental analyses were also obtained for compounds **1–5** after repeated column chromatographic purification and recrystallization. In addition, well-resolved ^{1}H NMR spectra (see Figs S1–S5) were recorded in DMSO-d_6 and the peak assignments could easily be made on the basis of integration and multiplicity of the signals.

UV-Vis spectra

Previously characterized zinc hydroxyphenylporphyrins were shown to exhibit a single Soret band and two Q bands [26], and this was also the case for the currently investigated compounds **1–5** in each solvent. Examples of spectra for compound **4** in CH_2Cl_2, DMF, DMSO or Py are given in Fig. 1 and a summary of the absorption peak maxima is given in Table 1.

Compound **4** exhibits a Soret band at 423 nm and two Q bands at 551 and 592 nm in the non-binding solvent CH_2Cl_2, and all three bands are red-shifted by 6–17 nm when the solvent is changed to DMF, DMSO or Py. As seen in the table, the Soret band is located at 429 nm in DMF, 432 nm in DMSO and 434 nm in Py while the Q bands are located at 562 and 604 nm in DMF, 564 and 605 nm in DMSO and 568 and 609 nm in Py, respectively. The relative intensity of the two Q bands varies with the solvent, but similar values are obtained in DMF, DMSO and Py as shown in Fig. 1 for the case of **4**, where the ratio of the absorbance of the two Q bands, $A_{Q(1,0)}/A_{Q(0,0)}$, is the value of 3.30 in the non-binding solvent CH_2Cl_2. As compared to 1.30 in DMF, 1.26 in DMSO and 1.11 in Py, where [(*p*-HOPh)$_3$(*p*-*t*BuPh)P]Zn(S) is generated as shown in Eq 1.

$$[(p\text{-HOPh})_n(p\text{-}t\text{BuPh})_{4-n}\text{P}]\text{Zn} + \text{S} \rightleftharpoons [(p\text{-HOPh})_n(p\text{-}t\text{BuPh})_{4-n}\text{P}]\text{Zn(S)} \quad (1)$$

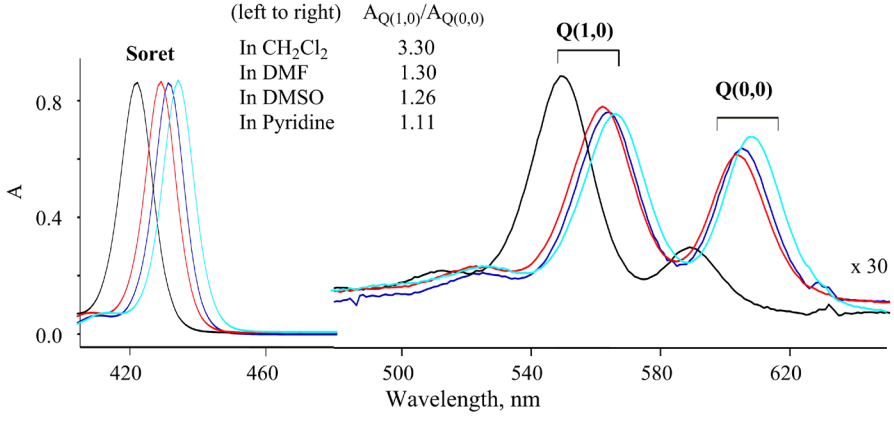

Fig. 1. UV-visible spectra of [(*p*-HOPh)$_3$(*p*-*t*BuPh)P]Zn **4** in different solvents

Table 1. UV-vis spectral data (λ_{max}, nm) of compounds **1–5** in different solvents

Solvent	Compound	Soret band	Q-band	
DCM	[(*p*-*t*BuPh)$_4$P]Zn **1**	421	549	589
	[(*p*-HOPh)(*p*-*t*BuPh)$_3$P]Zn **2**	422	550	590
	[*cis*-(*p*-HOPh)$_2$(*p*-*t*BuPh)$_2$P]Zn **3**	423	551	591
	[(*p*-HOPh)$_3$(*p*-*t*BuPh)P]Zn **4**	423	551	592
	[(*p*-HOPh)$_4$P]Zn **5**	424	552	593
DMF	[(*p*-*t*BuPh)$_4$P]Zn **1**	426	560	601
	[(*p*-HOPh)(*p*-*t*BuPh)$_3$P]Zn **2**	427	560	602
	[*cis*-(*p*-HOPh)$_2$(*p*-*t*BuPh)$_2$P]Zn **3**	428	561	603
	[(*p*-HOPh)$_3$(*p*-*t*BuPh)P]Zn **4**	429	562	604
	[(*p*-HOPh)$_4$P]Zn **5**	430	563	605
DMSO	[(*p*-*t*BuPh)$_4$P]Zn **1**	429	562	602
	[(*p*-HOPh)(*p*-*t*BuPh)$_3$P]Zn **2**	430	563	603
	[*cis*-(*p*-HOPh)$_2$(*p*-*t*BuPh)$_2$P]Zn **3**	431	564	604
	[(*p*-HOPh)$_3$(*p*-*t*BuPh)P]Zn **4**	432	564	605
	[(*p*-HOPh)$_4$P]Zn **5**	433	565	606
Py	[(*p*-*t*BuPh)$_4$P]Zn **1**	431	565	606
	[(*p*-HOPh)(*p*-*t*BuPh)$_3$P]Zn **2**	432	566	607
	[*cis*-(*p*-HOPh)$_2$(*p*-*t*BuPh)$_2$P]Zn **3**	433	567	608
	[(*p*-HOPh)$_3$(*p*-*t*BuPh)P]Zn **4**	434	568	609
	[(*p*-HOPh)$_4$P]Zn **5**	435	569	610

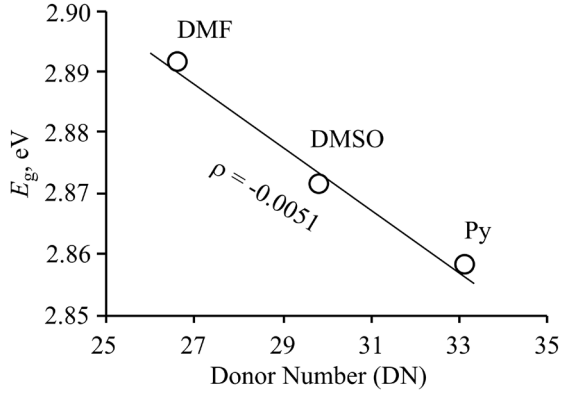

Fig. 2. Plot of the Soret band energy (E_g, eV) for [(*p*-HOPh)$_3$(*p*-*t*BuPh)P]Zn **4** *vs.* the Gutmann Donor Number (DN) of solvents

The changes in Soret band position with changes in the solvent can be quantitatively described by correlations between the energy (E_g, eV) of the Soret band and the Gutmann donor number (DN) of the solvent [23]. As shown in Fig. 2, a linear correlation is observed for compound **4** between the Soret band energy (E) and the DN of the three binding solvents. Similar linear correlations were observed for the other four investigated compounds, consistent with the fact that the red shift of the Soret band maxima and the relative intensity of the two Q bands in a given solvent both depend upon the presence or absence of solvent axial ligand binding to the Zn(II) center [24, 27, 28].

The position of the Soret absorption bands and the ratio of absorbances for the two Q bands of the porphyrin are also both dependent upon the type and position of substituents on the macrocycle. As seen in Table 1 and Fig. 3, the porphyrin Soret bands in DMSO (at 429 nm for **1** and 433 nm for **5)** undergo a systematic shift towards larger wavelengths with sequential increases in the sum of the Hammett substituent constants ($\Sigma\sigma$) for groups at the *para*-positions of the *meso*-phenyl rings. Fig. 4 shows the plot of the Soret band energy (E_g, eV) *vs.* the sum of the Hammett substituent constants for compounds **1–5** in DMSO. The ratio of the Q(1,0)/Q(0,0) band intensity is 1.63 in DMSO for the porphyrin lacking OH substituents and decreases to 1.59, 1.34, 1.26 and 1.17 upon a stepwise increase in the number of the HO groups on the *meso*-phenyl rings of the macrocycle.

Solvent binding reactions

Spectral titration methods were utilized to characterize solvent binding to the Zn(II) center of the porphyrin, and examples of the UV-vis spectral changes

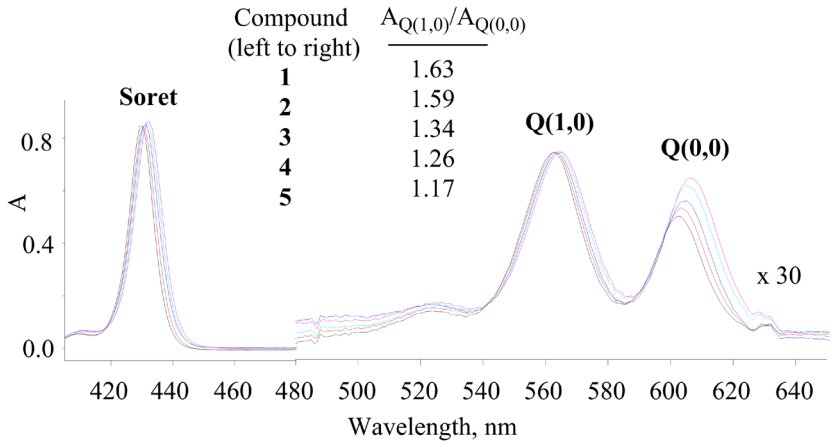

Fig. 3. UV-visible spectra of compounds **1–5** in DMSO

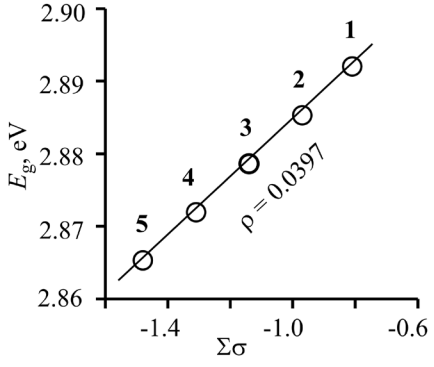

Fig. 4. Plot of the Soret band energy (E_g, eV) *vs.* the sum of the Hammett substituent constants (Σσ) for compounds **1–5** in DMSO

which occurred for compound **2** during titration with DMF, DMSO or Py in CH_2Cl_2, are shown in Fig. 5. These spectral changes were analyzed as a function of the solvent concentration at each step of the titration and this enabled calculation of the log*K* for solvent binding along with the number of axially bound solvent molecules using the Hill equation. For example, a diagnostic analysis plot of the measured absorption at 427 nm is shown in Fig. 5a, where a plot of $\log[(A_i-A_o)/(A_f-A_i)]$ *vs.* log[DMF] is linear with a slope of 1.0, indicating that a single DMF molecule is added in a one-step process to give the five-coordinate [(*p*-HOPh)(*p*-*t*BuPh)$_3$P]Zn(DMF) as the final porphyrin product. A solvent binding constant of log*K* = 1.63 was then calculated from the zero intercept of this plot. Similar spectral changes were obtained during the titration of **2** with DMSO (Fig. 5b) or pyridine (Fig. 5c) and a five-coordinate species is formed in each case, with log*K* = 2.46 for [(*p*-HOPh)(*p*-*t*BuPh)$_3$P]Zn(DMSO) and 3.71 for [(*p*-HOPh)-(*p*-*t*BuPh)$_3$P]Zn(Py).

Similar changes in the UV-vis spectra were observed for the four other porphyrins when DMF, DMSO or Py was added stepwise to a CH_2Cl_2 solution of the compound. The log*K* values were calculated using the standard equations, and a summary of the solvent binding constants is given in Table 2. In each case the final porphyrin products of the titration are characterized by a red-shifted Soret band and two red-shifted Q-bands as compared to the initial porphyrin in CH_2Cl_2. These types of spectral changes are typical for formation of five-coordinate Zn(II) porphyrins in nonaqueous media [24].

The magnitude of the solvent binding constants for (OEP)Zn, (OEP)FeCl and (OEP)MnCl were previously shown to correlate with the Gutmann solvent donor numbers [24], and this was also the case for the currently investigated zinc porphyrins, an example of which is shown in Fig. 6 for compound **2**.

The magnitude of the binding constant, log*K*, should also be related to the sum of the Hammett constants (Σσ) for groups at the *para*-positions of the four phenyl rings. For example, in a previously investigated series of (*p*-X)TPPCo derivatives (X = OCH_3, CH_3, H, F, Cl, CN and NO_2) [29], a larger solvent binding constant was observed in solvents with larger Hammett constants, while smaller solvent binding constants were observed for compounds whose substituents had smaller Hammett constants. Thus, the log*K* for solvent binding constant was expected to decrease upon going from compound **1** to **5** in each investigated solvent. This is indeed the case, as shown in Table 2 and Fig. 7.

Electrochemistry

The electrochemistry of each porphyrin was examined in four nonaqueous solvents containing 0.1 M TBAP as supporting electrolyte. Half-wave potentials for oxidation and reduction in each solvent are summarized in Table 3 and examples of cyclic voltammograms are illustrated in Figs 8 and 9.

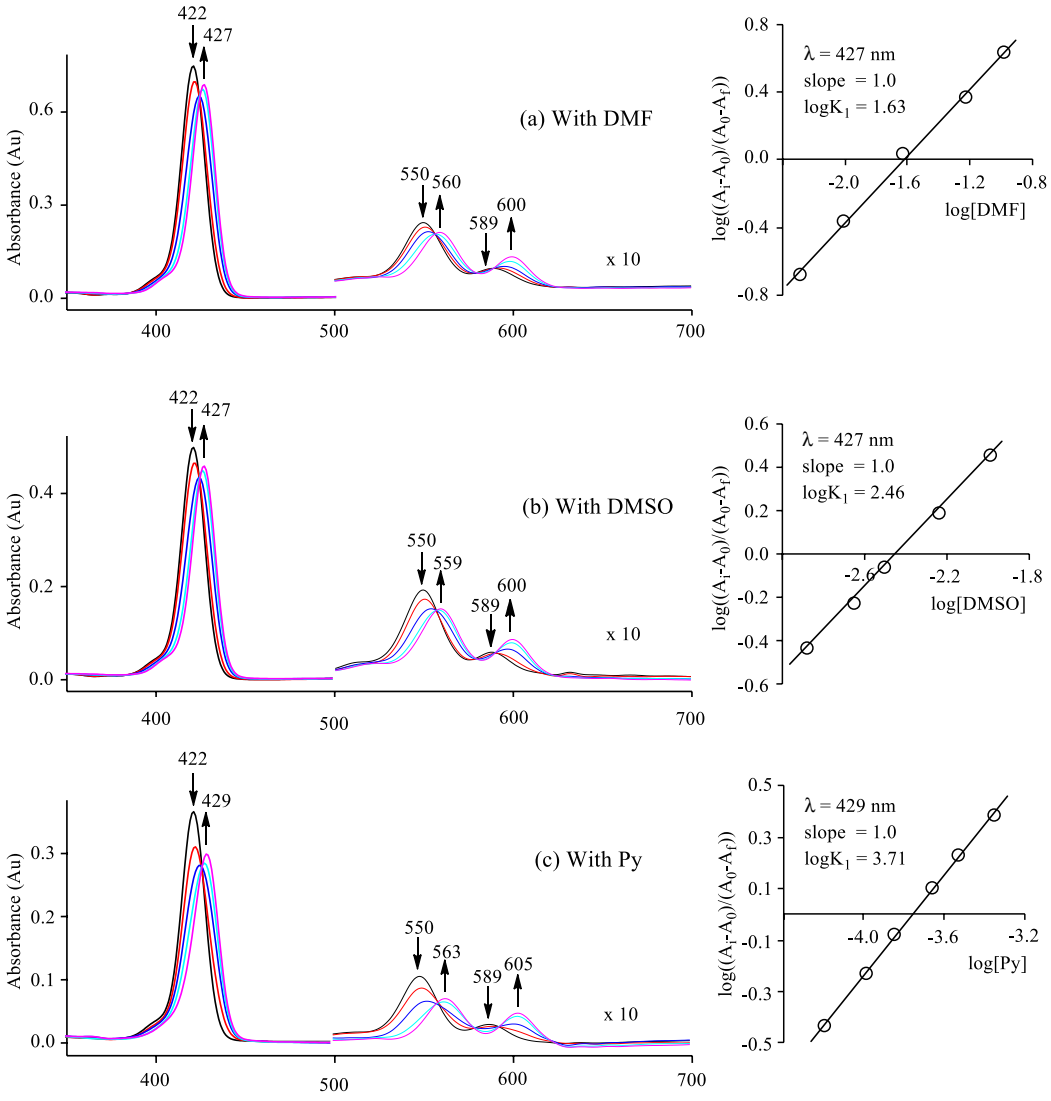

Fig. 5. UV-visible spectral changes during a titration of [(*p*-HOPh)(*p*-*t*BuPh)$_3$P]Zn **2** with (a) DMF, (b) DMSO and (c) Py in CH_2Cl_2. The insets are the Hill plots used to calculate the binding constants

Table 2. Solvent binding constants (log*K*) of compounds **1–5** in CH_2Cl_2

Compound	Σσ	Binding constants (log*K*)		
		DMF	DMSO	Py
[(*p*-*t*BuPh)$_4$P]Zn **1**	-0.80	1.65	2.49	3.73
[(*p*-HOPh)(*p*-*t*BuPh)$_3$P]Zn **2**	-0.97	1.63	2.46	3.71
[*cis*-(*p*-HOPh)$_2$(*p*-*t*BuPh)$_2$P]Zn **3**	-1.14	1.60	2.43	3.69
[(*p*-HOPh)$_3$(*p*-*t*BuPh)P]Zn **4**	-1.31	1.57	2.40	3.67
[(*p*-HOPh)$_4$P]Zn **5**	-1.48	1.55	2.36	3.65

The zinc metal center is electroinactive in the investigated compounds and each porphyrin undergoes two ring-centered reductions in CH_2Cl_2, DMSO and Py. However, an additional reduction is observed in DMF at much more negative potentials. The first reduction of **1–5** to give a π-anion radical is reversible in each solvent, but the second one-electron reduction is followed by a fast chemical reaction providing a species which can be reversibly reduced by one electron at more negative potentials. A third reduction was not observed for

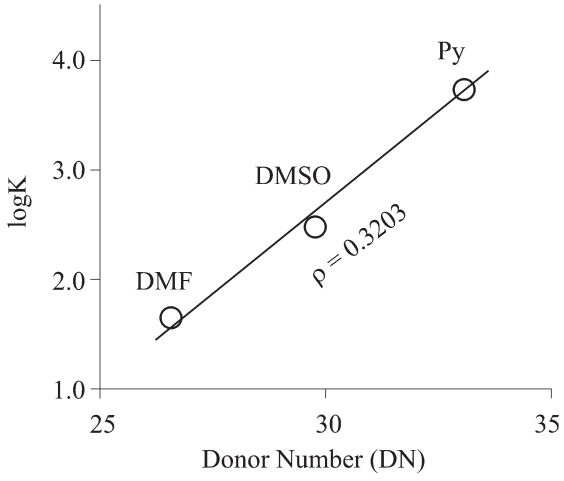

Fig. 6. Plot of the binding constants (log*K*) *vs.* the Gutmann Donor Number (DN) of the solvents (DMF = 26.6, DMSO = 29.8, Py = 33.1) for compound **2** in CH_2Cl_2

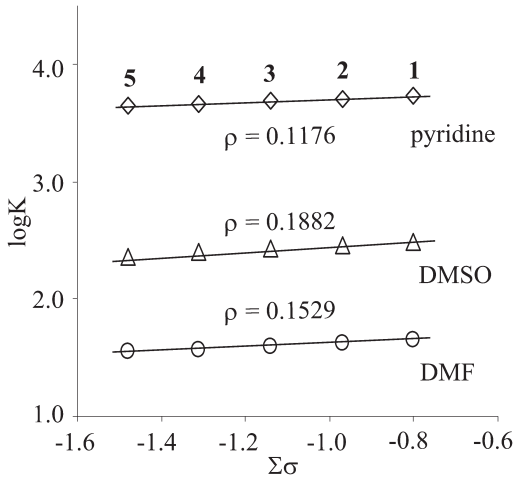

Fig. 7. Plots of the binding constants (log*K*) *vs.* the sum of the Hammett substituent constants (Σσ) for the addition of DMF, DMSO and pyridine to zinc porphyrins **1–5** according to Equation 1

compounds **1–5** in other solvents but it should be noted that compound **5** in DMSO also exhibits three one-electron reduction processes.

Fig. 8 illustrates the cyclic voltammograms obtained for compound **3** in the four utilized solvents. The first reduction is located at $E_{1/2}$ = -1.40 V in CH_2Cl_2,

Table 3. Half-wave potentials (V *vs.* SCE) of compounds **1–5** in different solvents containing 0.1 M TBAP

Compound	Solvent	Oxidation			Reduction		
		3rd	2nd	1st	1st	2nd	3rd
[(*p*-*t*BuPh)$_4$P]Zn **1**	CH_2Cl_2		1.04	0.71	-1.37	-1.86[a]	
	DMF			0.88[b]	-1.39	-1.82	-1.97
	DMSO			0.90[b]	-1.37	-1.75	
	Py			0.88[b]	-1.41	-1.90	
[(*p*-HOPh)(*p*-*t*BuPh)$_3$P]Zn **2**	CH_2Cl_2	1.56	0.99	0.69	-1.40	-1.80[a]	
	DMF			0.82[b]	-1.42	-1.81	-2.02
	DMSO			0.85[b]	-1.38	-1.78	
	Py			0.81[b]	-1.42	-1.90	
[*cis*-(*p*-HOPh)$_2$(*p*-*t*BuPh)$_2$P]Zn **3**	CH_2Cl_2	1.51	0.97	0.67	-1.40	-1.73[a]	
	DMF			0.81[b]	-1.41	-1.82	-2.06
	DMSO			0.82[b]	-1.39	-1.82	
	Py			0.82[b]	-1.43	-1.90	
[(*p*-HOPh)$_3$(*p*-*t*BuPh)P]Zn **4**	CH_2Cl_2	1.58[b]	0.97	0.67	-1.49	-1.84[a]	
	DMF			0.78[b]	-1.43	-1.83	-2.09
	DMSO			0.80[b]	-1.42	-1.82	
	Py			0.82[b]	-1.46	-1.95[a]	
[(*p*-HOPh)$_4$P]Zn **5**	CH_2Cl_2	1.60[b]	0.93	0.65	-1.49	-1.95[a]	
	DMF			0.78[b]	-1.42	-1.79	-2.15[a]
	DMSO			0.78[b]	-1.43	-1.82	-2.13[a]
	Py			0.70[b]	-1.47	-1.93	

[a]The irreversible reduction peak potentials, $E_{pc.}$
[b]The irreversible oxidation peak potentials, E_{pa}.

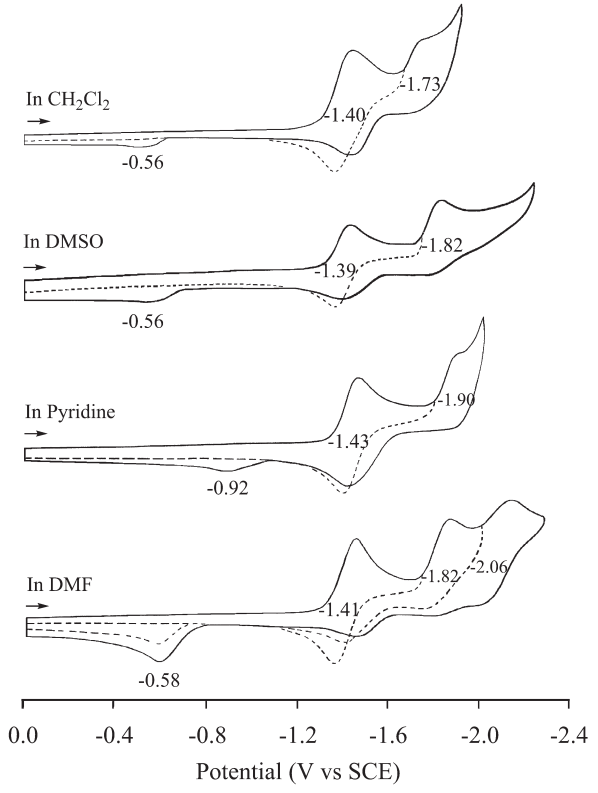

Fig. 8. Cyclic voltammograms showing reductions of compound **3** in CH_2Cl_2, DMSO, pyridine and DMF containing 0.1 M TBAP

-1.41 V in DMF, -1.39 V in DMSO and -1.43 V in pyridine. Thus, almost identical $E_{1/2}$ values are obtained for the first reversible one-electron addition, indicating that solvent coordination has only a small effect on half-wave potentials for first ring-centered reduction under the given solution conditions. The second reduction of compound **3** is associated with a coupled chemical reaction and a reoxidation at E_{pa} = -0.56 to -0.58 V in CH_2Cl_2, DMSO or DMF but at -0.92 V in Py. The irreversibility of the second reduction is associated with formation of a phlorin anion from the porphyrin dianion as earlier reported in the literature for (TPP)Zn in DMF [30, 31]. The assignment was confirmed in the present study by spectroelectrochemistry which is described below. As shown in Fig. 8, the product of the chemical reaction for compound **3** in DMF is reversibly reduced at -2.06 V.

A single irreversible oxidation of compounds **1–5** is observed in DMF, DMSO or Py, while two or three reversible oxidations are seen in CH_2Cl_2, the exact number depending upon the presence of OH substituents on the *meso*-phenyl positions of the porphyrin. Compound **1**, which lacks a hydroxyphenyl substituent, undergoes two reversible macrocycle-centered oxidations at $E_{1/2}$ = 0.71 and 1.04 V in CH_2Cl_2 containing 0.1 M TBAP (Fig. 9). These oxidations have been shown to generate the porphyrin π-cation radical and dication.

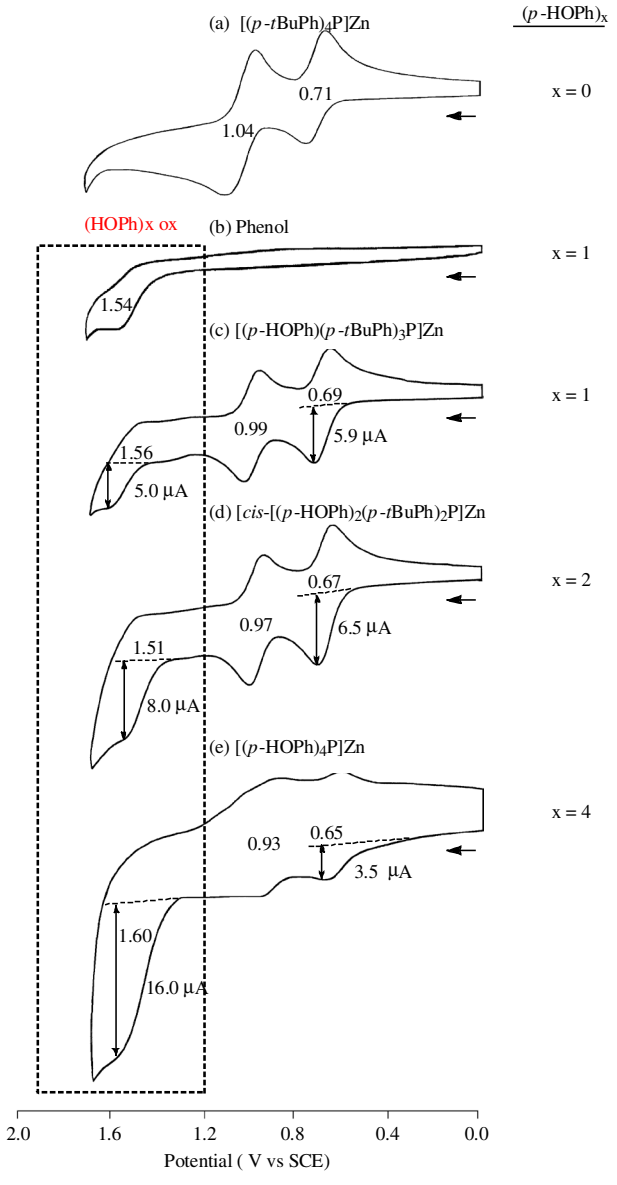

Fig. 9. Cyclic voltammograms showing oxidations of compounds **1**, **2**, **3** and **5** in CH_2Cl_2 containing 0.1 M TBAP

Similar oxidations are seen for compounds **2–5** but with the potentials shifted negatively due to the electron-donating hydroxyphenyl groups. A linear relationship is observed between the half-wave potential for the first or second oxidation and the sum of the Hammett substituents constant (Σσ), as shown in Fig. 10. In addition, one new oxidation process is observed for compounds **2–5** at potentials of 1.51 to 1.60 V. These processes are shown within a dotted box in Fig. 9 and involve the electroactive hydroxyphenyl groups on the *meso*-positions of the porphyrin.

The oxidation of phenol in CH_2Cl_2 is also shown in Fig. 9. This quasi-reversible process is located at $E_{1/2}$ = 1.54 V and is at an almost identical half-wave potential as for oxidation of the hydroxyphenyl groups on compounds **2** ($E_{1/2}$ = 1.56 V), **3** ($E_{1/2}$ = 1.51 V) and **5**

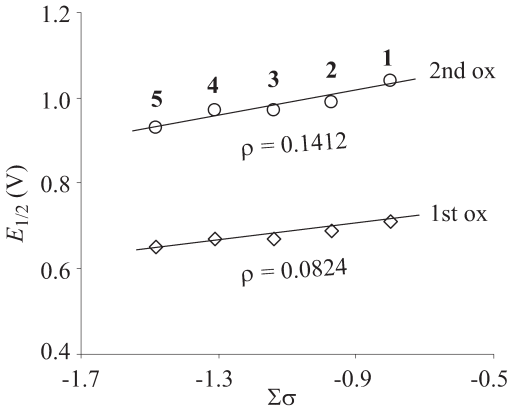

Fig. 10. Half-wave potentials of the first and second oxidations for compounds **1–5** in CH_2Cl_2 containing 0.1 M TBAP *vs.* the sum of the Hammett substituent constants (Σσ)

(E_{pa} = 1.60 V) under the same solution conditions. The peak current for oxidation of the one hydroxyphenyl group of compound **2** at 1.56 V is the same as that for the first or second ligand-based oxidations at 0.69 and 0.99 V. This is consistent with a one-electron transfer process in each step. In contrast, the peak current for oxidation of the two hydroxyphenyl groups of compound **3** (x = 2) at 1.51 V is twice as high as that for the first or second ring-centered oxidation of the same compound at $E_{1/2}$ = 0.67 and 0.97 V. Likewise, the current for oxidation of the hydroxyphenyl groups in compound **5** (x = 4) is four times higher than the current for the first and second ring-centered oxidations at $E_{1/2}$ = 0.65 and 0.93 V. These results are consistent with a two-electron and four-electron addition to compounds **3** and **5**, respectively, in the third oxidation step.

Detailed electrochemical studies of *meso*- and/or *β*-substituted porphyrins and corroles have shown that a larger substituent effect is often observed for reductions than for oxidations at the π-ring system of the compound [32, 33]. The first oxidation and first reduction potentials of [(*p*-HOPh)$_n$(*p*-*t*BuPh)$_{4-n}$P]Zn also appear to follow this trend (see Table 3). For example, the half-wave potential for the first reduction of [(*p*-HOPh)$_4$P]Zn **5** ($E_{1/2}$ = -1.49 V) in CH_2C1_2 is negatively shifted by 120 mV as compared to the first reduction of [(*p*-*t*BuPh)$_4$P]Zn **1** ($E_{1/2}$ = -1.37 V) in the same solvent, while the negative shift in $E_{1/2}$ for the first oxidation is only 60 mV upon going from compound **1** to compound **5** in CH_2C1_2.

Spectroelectrochemistry

Examples of the thin-layer UV-visible spectra obtained during the first and second reductions of [*cis*-(*p*-HOPh)$_2$(*p*-*t*BuPh)$_2$P]Zn **3** in DMF containing 0.1 M

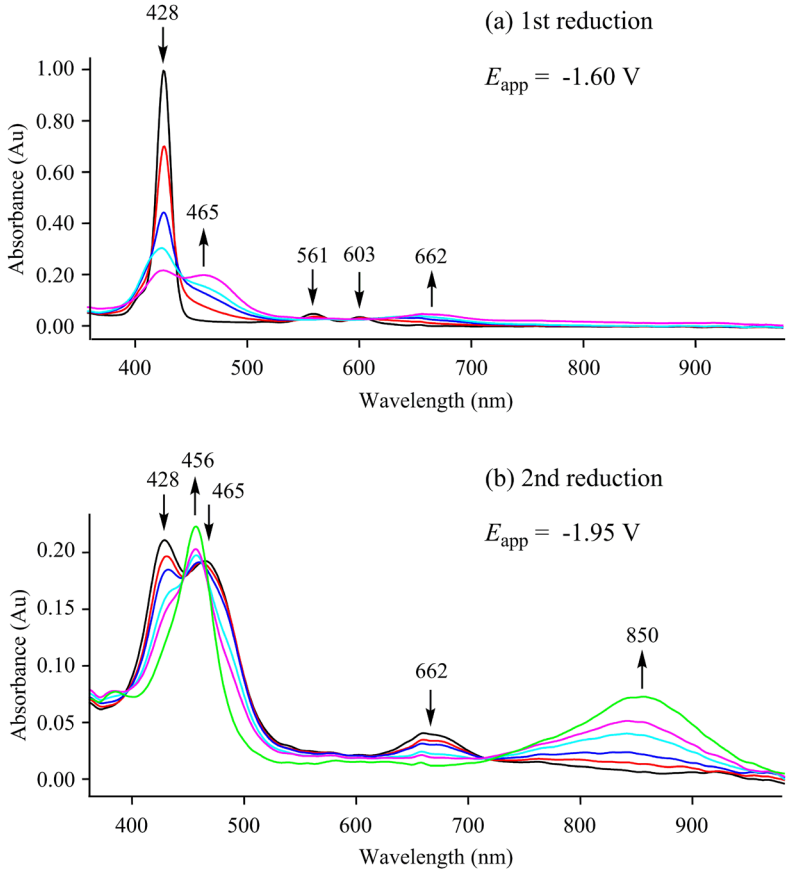

Fig. 11. UV-vis spectral changes of [*cis*-(*p*-HOPh)$_2$(*p*-*t*BuPh)$_2$P]Zn **3** during the (a) first and (b) second reductions in DMF, 0.1 M TBAP

TBAP are shown in Fig. 11. As seen from this figure, the Soret band at 428 nm decreases significantly in intensity upon applying a controlled reducing potential of E_{app} = -1.60 V, while a new band grows in at 465 nm (Fig. 11a). At the same time the two bands at 561 and 603 nm completely disappear and a new broad band characteristic of a porphyrin π-anion radical appears at 662 nm. This reduction is reversible, and the original electronic absorption spectrum of the neutral compound could be regenerated upon reoxidation of the singly reduced species at a position potential.

During the second reduction of [*cis*-(*p*-HOPh)$_2$(*p*-*t*BuPh)$_2$P]Zn **3** at an applied potential of E_{app} = -1.95 V (Fig. 11b), the porphyrin bands at 428, 465 and 662 nm disappear as new absorption bands grow in at 456 and 850 nm. The latter band is characteristic of a phlorin anion and is similar to what has been reported for the electrogenerated phlorin dianions of (TPP)Zn and (TPP)H_2 in DMF, 0.1 M TBAP [30, 31] or (Ph)$_2$(P(O)(OEt)$_2$)$_2$PorM (M = Cu, Ni, Pd) in PhCN, 0.1 M TBAP [34].

CONCLUSIONS

The electrochemical and spectroelectrochemical properties of four zinc *p*-hydroxylphenyl porphyrins were investigated in CH_2Cl_2, DMF, DMSO and pyridine. The effects of the solvent and *meso*-phenyl ring substituents on the UV-vis spectra are quantitatively described by shifts in the energy of the Soret band *vs.* the Gutmann solvent donor number (DN) or the sum of the Hammett constants of the substituents (Σσ) at the *para*-positions of the macrocycle. Solvent binding constants (log*K*) were also determined for the *in situ* generated five-coordinate complex [(*p*-HOPh)$_n$ (*p*-*t*BuPh)$_{4-n}$P]Zn(S).

The investigated compounds undergo two ring-centered reductions, the second of which is followed by a chemical reaction of the porphyrin dianion to give an anionic phlorin product. The phlorin anion is reversibly reduced by one electron at a more negative potential to give a phlorin dianion in DMF. Each porphyrin also undergoes two ring-centered one-electron oxidations, leading to formation of a π-cation radical and dication in CH_2Cl_2 containing 0.1 M TBAP. An additional oxidation process is also observed for compounds **2–5** which involves the redox active hydroxyphenyl groups on the *meso*-positions of the porphyrin.

Acknowledgments

We gratefully acknowledge support from the National Natural Science Foundation of China (Grant No. 21001054), the Foundation of Jiangsu University (Grant No. FCJJ2015020, 05JDG051) and the Robert A. Welch Foundation (K.M.K., Grant E-680).

Supporting information

^{1}H NMR spectra in DMSO-d_6 for compounds **1–5** is given in the supplementary material. This material is available free of change *via* the Internet at http://worldscinet.com/jpp/jpp.shtml.

REFERENCES

1. Dzieciuch M, Rissanen S, Szydlowska N, Bunker A, Kumorek M, Jamroz D, Vattulainen I, Nowakowska M, Rog T and Kepczynski M. *J. Phys. Chem. B* 2015; **119**: 6646–6657.
2. Wikene KO, Bruzell E and Toennesen HH. *J. Photochem. Photobiol. B* 2015; **148**: 188–196.
3. Hamed B, Haimberger TV, Kozich V, Wiehe A and Heyne K. *J. Photochem. Photobiol. A* 2014; **295**: 53–56.
4. Serra A, Pineiro M, Santos CI, Gonsalves AMdAR, Abrantes M, Laranjo M and Botelho MF. *Photochem. Photobiol.* 2010; **86**: 206–212.
5. Ibrahim H, Kasselouri A, Raynal B, Pansu R and Prognon P. *J. Lumin.* 2011; **131**: 2528–2537.
6. Wang Y, Hu Y, Wu T, Liu H, Zhang L, Zhou X and Shao Y. *Analyst* 2015; **140**: 5169–5175.
7. Jiang L, Li M, Lin L, Li Y, He X, Cui L. *RSC Adv.* 2014; **4**: 26653–26661.
8. Yuan B, Ge R, Kang S-Z, Qin L, Li G and Li X. *RSC Adv.* 2015; **5**: 94046–94052.
9. Bian Y, Chen X, Wang D, Choi C-F, Zhou Y, Zhu P, Ng DKP, Jiang J, Weng Yand Li X. *Chem.-Eur. J.* 2007; **13**: 4169–4177.
10. Lu G, Zhang X, Cai X and Jiang J. *J. Mater. Chem.* 2009; **19**: 2417–2424.
11. Lu G, Chen Y, Zhang Y, Bao M, Bian Y, Li X and Jiang J. *J. Am. Chem. Soc.* 2008; **130**: 11623–11630.
12. Lu G, Ou Z, Jiang J and Bian Y. *Eur. J. Inorg. Chem.* 2010; 753–757.
13. Dogan N, Dumanogullari FM, Hayvali M, Yilmaz H, Kueruem U, Yaglioglu HG and Elmali A. *Chem. Phys. Lett.* 2011; **508**: 265–269.
14. Seidel RW, Goddard R and Oppel IM. *CrystEngComm.* 2014; **16**: 10505–10511.
15. Smykalla L, Shukrynau P, Mende C, Lang H, Knupfer M and Hietschold M. *Chem. Phys.* 2015; **450–451**: 39–45.
16. Hill JP, Wakayama Y, Akada M and Ariga K. *J. Phys. Chem. C* 2007; **111**: 16174–16180.
17. Lu G, Zhang X, Cai X, Fang Y, Zhu M, Zhu W, Ou Z and Kadish KM. *J. Porphyrins Phthalocyanines* 2013; **17**: 941–953.
18. De Luca G, Romeo A and Scolaro LM. *J. Phys. Chem. B* 2006; **110**: 14135–14141.
19. Guo H, Jiang J, Shi Y, Wang Y, Wang Y and Dong S. *J. Phys. Chem. B* 2006; **110**: 587–594.

20. Savenije TJ, Koehorst RBM and Schaafsma TJ. *J. Phys. Chem. B* 1997; **101**: 720–725.
21. Kadish KM, Larson G, Lexa D and Momenteau M. *J. Am. Chem. Soc.* 1975; **97**: 282–288.
22. Evans TA, Srivatsa GS, Sawyer DT and Traylor TG. *Inorg. Chem.* 1985; **24**: 4733–4735.
23. Gutmann V and Wychera E. *Monatsh. Chem.* 1965; **96**: 828–835.
24. Zhu W, Zhao X, Ou Z, Zhou F, Wang X and Kadish KM. *J. Porphyrins Phthalocyanines* 2009; **13**: 1233–1242.
25. Adler AD, Longo FR, Kampas F and Kim J. *J. Inorg. Nucl. Chem.* 1970; **32**: 2443–2445.
26. Brückner C, Samankumara L and Ogikubo J. In *Handbook of Porphyrin Science*, Kadish KM, Smith KM, Guilard R (Ed.), World Scientific: River Edge, New York, 2012, Vol. 17, Ch. 76, pp. 1–112.
27. Nappa M and Valentine JS. *J. Am. Chem. Soc.* 1978; **100**: 5075–5080.
28. Spellane PJ, Gouterman M, Antipas A, Kim S and Liu YC. *Inorg. Chem.* 1980; **19**: 386–391.
29. Walker FA, Beroiz D and Kadish KM. *J. Am. Chem. Soc.* 1976; **98**: 3484–3489.
30. Lanese JG and Wilson GS. *J. Electrochem. Soc.* 1972; **119**: 1039–1043.
31. Wilson GS and Peychal-Heiling G. *Anal. Chem.* 1971; **43**: 545–550.
32. Kadish KM, Van Caemelbecke E and Royal G. In *The Porphyrin Handbook*, Kadish KM, Smith KM, Guilard R. (Ed.), Academic Press: New York, 2000, Vol. 8, Ch. 55, pp. 1–114.
33. Fang Y, Ou Z and Kadish KM. *Chem. Rev*. 2017; **117**: 3377–3419.
34. Fang Y, Gorbunova YG, Chen P, Jiang X, Manowong M, Sinelshchikova AA, Enakieva YY, Martynov AG, Tsivadze AY, Bessmertnykh-Lemeune A, Stern C, Guilard R and Kadish KM. *Inorg. Chem.* 2015; **54**: 3501–3512.